ACCURATE 3D PSF ESTIMATION FROM A WIDE-FIELD MICROSCOPY IMAGE

Jizhou Li[1]*, Feng Xue*[2]*, and Thierry Blu*[1]

[1] Department of Electronic Engineering, The Chinese University of Hong Kong, Hong Kong
[2] National Key Laboratory of Science and Technology on Test Physics and Numerical Mathematics, Beijing, China

ABSTRACT

The 3D point-spread function (PSF) plays a fundamental role in wide-field fluorescence microscopy. An accurate PSF estimation can significantly improve the performance of deconvolution algorithms. In this work, we propose a calibration-free method to obtain the PSF directly from the image obtained. Specifically, we first parametrize the spherically aberrated PSF as a linear combination of few basis functions. The coefficients of these basis functions are then obtained iteratively by minimizing a novel criterion, which is derived from the mixed Poisson-Gaussian noise statistics. Experiments demonstrate that the proposed approach results in highly accurate PSF estimations.

***Index Terms*—** point-spread function, wide-field microscopy, parametric PSF estimation, 3D deconvolution microscopy

1. INTRODUCTION

Three-dimensional (3D) wide-field fluorescence microscopy is widely used to analyze the structures of living biological specimens. Different from the confocal laser scanning microscopy, which scans the sample point-by-point, a stack of 2D images recorded from different focus planes along the optical axis is collected to represent the 3D information. While wide-field microscopy has the advantage of fast acquisition and low light exposure, which is suitable for live cell imaging, the acquired images are often blurred because of out-of-focus contributions [1, 2]. This is especially true when imaging thicker samples (those thicker than about 15 to 30 μm). Image deconvolution provides a computational technique to mitigate this distortion by using information describing how the microscope produces the image and reassigns the out-of-focus light to the points of origin [3–5].

The point spread function (PSF), which represents the impulse response of this imaging system to a point source or object, is essential for an accurate image deconvolution. In wide-field microscope, one of the main characteristics of the PSF is spherical aberration. It is caused by refractive-index mismatch between the immersion and specimen layers. One direct way for obtaining a 3D PSF is to image a point-like fluorescence bead, of a size smaller than the resolution of the system. However, such experimental PSFs involve noise and the imaging conditions of bead measurements are different from those in actual imaging.

The alternative would be to use an analytical model of the PSF, which takes into account the physical aberrations of the acquisition system [1, 6, 7]. The Gibson-Lanni model [6, 8, 9] is one of the most widely used PSF models for wide-field microscopy. It is based on Kirchhoff's integral formula, and generates a 3D PSF by substituting several optical parameters. Although the model-based PSF is noise-free, it is still not practical since some of the necessary parameters such as the refractive index of the specimen are difficult to obtain or might change due to heating of live samples during the course of the experiments.

It is thus preferable to estimate the PSF directly from the measurements. An accurate estimation can significantly improve the deconvolution performance, and is also beneficial to calibrate a microscope. Most algorithms bypass this problem by simultaneously estimating the PSF and the object, based on *prior* hypotheses on them [10–15]. Alternatively, we can perform the estimation of the PSF and the object separately. This way allows to carry out any high-quality non-blind deconvolution to obtain the original object [16,17].

In this work, the 3D microscopy PSF is parametrized as a linear combination of few basis functions. These basis functions are also derived from Kirchhoff's integral formula, thus automatically satisfy all the constraints imposed by the model. With an efficient algorithm, the PSF is obtained by minimizing a novel criterion. This criterion, the "blur-SPURE" (Stein-Poisson Unbiased Risk Estimate), is based on the mixed Poisson-Gaussian noise statistics [18] and extended from the blur-SURE [16] and blur-PURE criteria [17]. The paper is organized as follows: Section 2 introduces our approximation model for the PSF in the wide-field microscopy; we then describe the blur-SPURE criterion and present our algorithms for the PSF estimation in Section 3. Finally we present experimental results in Section 4 to illustrate the effectiveness of the proposed approach.

2. MICROSCOPY PSF APPROXIMATION

One of the advantages of the Gibson-Lanni model is that it can predict the non-symmetric patterns in the axial direction, which reflects the spherical aberration and often appears in realistic imaging conditions [6, 9]. This model is based on a calculation of the optical path difference (OPD) between experimental conditions and the design conditions of the objective. However, the Gibson-Lanni model depends on a large number of non-linear parameters, which renders it inadequate for a global optimization approach.

We propose to approximate the microscopy PSF by a linear combination of basis functions. For each basis function, the key idea is to simplify the OPD (corresponding to the phase) by a parametrized function $f_{ij}(\rho, z; \eta) = z\sqrt{n_i^2 - \rho^2} + \eta\sqrt{n_j^2 - \rho^2}$, where z is the axial coordinate of the focal plane, and ρ is the normalized radius in the focal plane. The (n_i, n_j) are akin to refractive indices, and their values are fixed once for all. The parameter η is an indication of the focus position z_p, but they are not necessarily to be equal in quantity. More specifically, the PSF h is written as a linear combination

This work was supported by grants from the Research Grants Council (RGC) of Hong Kong (AoE/M-05/12).

of basis functions as

$$h_{\text{app}}(\mathrm{r};\mathrm{c},\eta) = \sum_{i,j} c_{i,j}\, h_{i,j}(\mathrm{r};\eta), \tag{1}$$

where

$$h_{i,j}(\mathrm{r};\eta) = \left| A \int_0^{\min(\mathrm{NA},n_i,n_j)} \exp\Big(ik\, f_{i,j}(\rho,z;\eta)\Big) J_0\left(kr\rho\right) \rho \mathrm{d}\rho \right|^2,$$

$\mathrm{c} = \{c_{i,j}, i,j = 1,2\}$ are the coefficients of basis functions, n_i, n_j take values in $\{1.35, 1.45\}$ which are empirically determined, A is a constant complex amplitude, $k = 2\pi/\lambda$ is the wave number, $r = \|\mathrm{r}\|$ and J_0 denotes the Bessel function of the first kind of order zero. Each basis function $h_{i,j}(\mathrm{r};\eta)$ is computed efficiently using a fast approach based on Bessel series approximation in [9].

For the proposed parametrization, when the wavelength λ and NA are provided (which is usually the case), only the focus position η and 4 linear coefficients c have to be determined. The degrees of freedom is greatly reduced compared with the original Gibson-Lanni model.

Note that the linear approximation in (1) is different from the approaches in Markham et al. [11] and Soulez et al. [13], where the phase term of the original model is approximated by a linear combination of several (typically larger than 6) polynomials (either power or Zernike polynomials). The corresponding coefficients are thus highly non-linear and more difficult to estimate accurately since they are involved in an integral. The proposed parametrization is also distinct from the approach in [12], where the basis functions are learned from a training set of PSFs with different focus positions.

3. PSF ESTIMATION ALGORITHM

3.1. Image formation model

The wide-field fluorescence microscope can be modeled as a linear shift-invariant system, due to the incoherent nature of the emitted fluorescence light [3, 4]. The noise degradation is considered to be mixed Poisson-Gaussian as in [18]; i.e.,

$$\mathrm{y} = \alpha\, \mathcal{P}\left(\frac{\mathbf{H}_0\mathrm{x}}{\alpha}\right) + \mathcal{N}(0,\sigma^2\mathbf{I}), \tag{2}$$

where $\mathrm{y} \in \mathbb{R}^N$ denotes the distorted observation of the unknown 3D true original image $\mathrm{x} \in \mathbb{R}^N$, $N = N_x \times N_y \times N_z$ is the size of the measurement. The scalar α represents the gain of the measurement device, which controls the noise during the acquisition. $\mathbf{H}_0 \in \mathbb{R}^{N\times N}$ is a block-circulant matrix, which implements a discrete convolution with the PSF h[1]. $\mathbf{I}$ denotes the identity matrix, $\mathcal{P}(\cdot)$ and $\mathcal{N}(\cdot,\cdot)$ represent the effect of the Poisson noise and the additive Gaussian noise (variance σ^2), respectively. The values of α and σ^2 can be estimated by a robust linear regression performed on a collection of local estimates of the sample mean and variance [18, 19].

Based on the image acquisition model in (2), the objective of this work is to estimate the PSF h (namely $\mathbf{H}_0$) directly from the measurement y. This is a well-known difficult inverse problem since both the original image x and the PSF are unknown. However, the PSF parametrization in Section 2 greatly reduces the degrees of freedom.

[1] We do not consider space-varying PSFs in this paper.

3.2. Blur-SPURE as an optimization criterion

The PSF estimation, with respect to finding a set of coefficients in (1), can be done by minimizing the expected mean squared error (MSE) between the blurred image $\mathbf{H}_0\mathrm{x}$ and a linear processing of the measurement y [16, 17]. This oracle criterion (knowing $\mathbf{H}_0\mathrm{x}$) is named as *blur-MSE*. More specifically, our strategy consists in minimizing blur-MSE $= \frac{1}{N}\mathcal{E}\{\|\mathbf{U}_{\mathbf{H},\mu}\mathrm{y} - \mathbf{H}_0\mathrm{x}\|^2\}$, over $\mathbf{H}$ and μ, where $\mathbf{U}_{\mathbf{H},\mu} = \mathbf{H}\mathbf{H}^{\mathrm{T}}\Big(\mathbf{H}^{\mathrm{T}}\mathbf{H} + \mu\mathbf{P}\Big)^{-1}$ and μ is some positive scalar estimated by line search.

The matrix $\mathbf{U}_{\mathbf{H},\mu}$ corresponds to a filter whose frequency response can be thought as a kind of band-indicator since it marks a certain frequency band as 0 or 1 with a narrow transition between the two values. $\mathbf{P}$ is an approximation of the power density spectrum of the origin image x. It is often expressed by the discrete Laplacian operator ($\|\omega\|^2 = \omega_x^2 + \omega_y^2 + \gamma\,\omega_z^2$), where γ is the ratio between lateral and axial resolutions. It can be proven that for all $\mathbf{U}_{\mathbf{H},\mu}$, the solution $\mathbf{H}$ minimizing the *blur-MSE* is related to the true matrix $\mathbf{H}_0$, through $\mathbf{H}\mathbf{H}^{\mathrm{T}} = \mathbf{H}_0\mathbf{H}_0^{\mathrm{T}}$. Note that this means that the PSF will be retrieved up to a shift, which is not a big issue since a shift does not induce any distortion.

In practice we cannot minimize the *blur-MSE* directly since $\mathbf{H}_0\mathrm{x}$ is unknown. We then use an unbiased estimate of its expected value, blur-SPURE (Stein-Poisson Unbiased Risk Estimate), for the minimization. For the linear degradation model (2), we have the following theorem (similar to [16, 17]).

Theorem 1 *Consider the degradation model* (2) *and* $\mathbf{U}$ *an arbitrary matrix, the random variable*

$$\begin{aligned}\text{blur-SPURE}\{\mathbf{U}\} = {} & \frac{1}{N}\|\mathbf{U}\mathrm{y}\|^2 + \frac{1}{N}\|\mathrm{y}\|^2 - \frac{\alpha}{N}\mathbf{1}^{\mathrm{T}}\mathrm{y} \\ & - \frac{2}{N}\sum_{n=1}^{N} \mathrm{y}^{\mathrm{T}}\mathbf{U}(\mathrm{y} - \alpha\,\mathrm{e}_n) + \frac{2\sigma^2}{N}\mathrm{Tr}(\mathbf{U}) - \sigma^2,\end{aligned}$$

is an unbiased estimate of the blur-MSE; i.e., $\mathcal{E}\{\text{blur-SPURE}\} = \frac{1}{N}\,\mathcal{E}\left\{||\mathbf{U}\mathrm{y} - \mathbf{H}_0\mathrm{x}||^2\right\}$, *where* e_n *is the* N*-dimensional vector with components* $\delta_{k-n}, k = 1, 2, ..., N$*, and* N *is the number of pixels of the image.*

This criterion solely depends on the observed image y thus is computable. The statistical unbiasedness with the *blur-MSE* and the fact that the pixel number of the 3D image N is very large (typically, $256 \times 256 \times 32 = 2,097,152$) indicate that the blur-SPURE can be used as a reliable subsitute of the *blur-MSE* (law of large numbers). Note that all matrices involved are diagonalized by the discrete 2D Fourier transformation, and so, the blur-SPURE can be efficiently computed in the Fourier domain.

3.3. PSF estimation by band-indicator approximation

The optimization criterion, blur-SPURE, provides explicit control over the PSF estimation problem. However, direct minimizing the blur-SPURE cannot guarantee the optimal solution, which is mainly because this is a highly non-convex optimization problem that has many local minima. Instead, we propose to firstly approximate the true band-indicator $\mathbf{U}_{\mathbf{H}_0,\mu}$ by a linear combination of basis functions $\mathbf{U}_{\text{app}} = \sum_{i,j} \hat{c}_{i,j}\, \mathbf{U}_{\mathbf{H}_{i,j},\mu}$, where $\mathbf{H}_{i,j}$'s are constructed by the corresponding $h_{i,j}(\mathrm{r};\eta)$ as described in Section 2. Thanks to the quadratic nature of the blur-SPURE, the search for the optimal coefficients $\hat{\mathrm{c}} = \{\hat{c}_{i,j}, i,j = 1,2\}$ boils down to the solution of a linear system of equations. The parameter η is simultaneously obtained by line search within the thickness of the specimen.

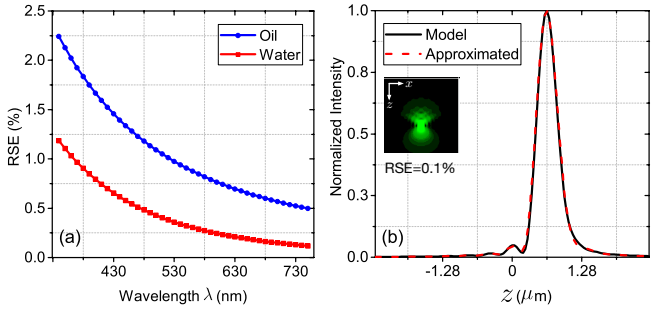

Fig. 1. (a) Plots of the mean RSEs under two different immersion mediums (water and oil) over various scenarios. (b) Axial intensity profile of typical PSFs ($\lambda = 492$ nm, $z_p = 750$ nm) generated by the complete Gibson-Lanni model (the black curve) and its approximation (the dashed red curve) by (1). Note the non-symmetric pattern caused by the refractive index mismatch.

Once $\mathbf{U}_{\text{app}}$ has been found, finding the PSF $\mathbf{H}$ amounts to solving the following unconstrained minimization problem: $\min_{\mathbf{H}} \|\mathbf{H}\mathbf{W}_{\mathbf{H}} - \mathbf{U}_{\text{app}}\|_2^2$, where $\mathbf{H}$ assumes the parametric expression (1) and $\mathbf{W}_{\mathbf{H}} = \mathbf{H}^{\mathrm{T}}(\mathbf{H}^{\mathrm{T}}\mathbf{H} + \mu\mathbf{P})^{-1}$. We propose an alternating optimization algorithm:

$$\mathbf{H}^{(k)} = \underset{\mathbf{H}=\sum_{i,j} c_{i,j}\mathbf{H}_{i,j}}{\arg\min} \|\mathbf{H}\mathbf{W}_{\mathbf{H}^{(k-1)}} - \mathbf{U}_{\text{app}}\|_2^2, \qquad (3)$$

where

$$\mathbf{W}_{\mathbf{H}^{(k-1)}} = \frac{\mathbf{H}^{(k-1)} + (\mathbf{H}^{(k-1)})^{\mathrm{T}}}{2}\left((\mathbf{H}^{(k-1)})^{\mathrm{T}}\mathbf{H}^{(k-1)} + \mu\mathbf{P}\right)^{-1},$$

and $\mathbf{H}^{(0)}$ is randomly initialized. The solution $\mathbf{H}^{(k)}$ involves finding the coefficients $c_{i,j}^{(k)}$'s by solving a linear system of equations at each iteration until $\|\mathbf{H}^{(k)} - \mathbf{H}^{(k-1)}\|/\|\mathbf{H}^{(k-1)}\| \le 10^{-3}$.

4. EXPERIMENT AND RESULTS

The PSF estimation performance is measured in terms of the relative squared error (RSE) [9,20] calculated as $\|h_{\text{app}} - h\|_2^2/\|h\|_2^2 \times 100\%$. Basically, the estimation is thought to be accurate when RSE $< 9\%$ [20].

4.1. Validation of the PSF parametrization model

To validate the proposed parametrization model in (1), we generate the ground truth PSFs based on the complete Gibson-Lanni model [6, 9] under different settings. Then the differences between the true PSFs and the fitted PSFs by (1) are evaluated. Specifically, we consider refractive indices n_s's of typical cellular components in the range from 1.354 to 1.5 with a step of 0.05. The wavelength λ is in the range from 340 nm to 750 nm with a step of 10 nm, which are frequently used in real experiments. Two different types of immersion media (water and oil) are used. Their refractive indices n_i's are 1.33 and 1.515 respectively. Other parameters are followed by the setting of a $63\times$ magnification, 1.4 NA Andor Zyla camera. The focus position z_p varies from $-1.5\,\mu$m to $1.5\,\mu$m with a step of $0.05\,\mu$m, which covers the range of expected spherical aberrations. There are totally $15,372$ PSFs of size $127 \times 127 \times 127$.

Fig. 1(a) shows the mean RSEs under water and oil medias with respect to the wavelength. The maximum value is 2.24%, which demonstrates the effectiveness of the proposed parameterization model. Note that PSFs with longer wavelength have lower frequency (less rings) thus relatively are more easily approximated.

Table 1. RSE (%) comparison of the PSF estimation accuracy with other approaches under different scenarios. The results have been averaged over 5 random initializations.

focus position	$z_p = 0$ nm		$z_p = 500$ nm		$z_p = 1500$ nm	
α, σ^2	0.02	0.2	0.02	0.2	0.02	0.2
Image	*Bars* $256 \times 256 \times 128$					
Blind R-L	45.05	54.67	291.37	290.63	454.24	548.49
AIDA [21]	88.75	109.64	121.48	399.36	231.20	323.92
fminsearch	5.80	19.39	13.46	74.43	20.72	114.69
Proposed	**1.26**	**2.98**	**3.52**	**4.80**	**5.26**	**5.77**
Image	*Pollen* $256 \times 256 \times 32$					
Blind R-L	16.73	35.09	16.93	63.97	38.77	147.70
AIDA [21]	44.65	45.51	104.79	106.86	122.32	160.05
fminsearch	1.45	8.12	1.67	19.59	20.76	64.64
Proposed	**0.88**	**2.70**	**1.47**	**3.70**	**3.04**	**4.72**

*Best estimation results are highlighted.

One typical example of a sample with refractive index 1.4 illuminated with green light (λ = 492nm) is shown in Fig. 1(b). The non-symmetric pattern caused by the refractive index mismatch can be well predicted by the proposed model.

4.2. Comparison with other approaches

We adapt the confocal image simulator in [22] to the wide-field settings. Three PSFs with different focus positions ($z_p = 0, 500, 1500$ nm respectively) are generated according to the Gibson-Lanni model with typical values for the parameters ($\lambda = 492$nm, NA=1.4, $n_i = 1.33, n_s = 1.4$). The pixel size is 100 nm in the x-y plane and 250 nm along the z-axis. Two original images, *Bars* and *Pollen* [5], are convolved with these PSFs. The blurred images are subsequently contaminated by mixed Poisson-Gaussian noise with different noise levels (corresponding to different α and σ^2 values). Typically, we obtain a low noise image when $\alpha = 0.02, \sigma^2 = 0.02$ and a high noise image when $\alpha = 0.2, \sigma^2 = 0.2$.

We compare with the popular blind deconvolution methods (the blind Richardson-Lucy algorithm [23, 24] and AIDA [21]). To demonstrate the effectiveness of the iterative algorithm in (3), the alternative scheme using the *fminsearch* in Matlab is also evaluated. Note that all estimated PSFs are optimally shifted in the z-axis to best match the ground-truth PSF.

Table 1 presents the RSEs between the estimated and ground-truth PSFs over different scenarios. It can be seen that the proposed approach generally yields significantly more accurate and consistent PSF estimation than other methods. Two typical cases are shown in Fig. 2. The proposed approach succeeds in estimating the spherical aberration of the PSF. The iterative algorithm in (3) generally converges within less than 50 iterations. Each iteration takes $\sim$0.27s for the *Pollen* image and $\sim$1.15s for the *Bars* image. Note that our main goal is to evaluate the estimated PSFs instead of the deconvolved images: we believe that accurate PSF estimation conveys valuable additional information about the sample and the microscope setting.

5. CONCLUSION

We proposed a 3D PSF estimation method for wide-field fluorescence microscopy. We characterized the PSF by a linear combination of few basis functions, and introduced a novel criterion based on the mixed Poisson-Gaussian noise statistics, namely blur-SPURE, for the optimization. In conjunction with an iterative algorithm, the proposed algorithm yields significantly more accurate PSF estimations than other approaches. Future works include applying the technique to the microscope calibration [25] and blind depth-variant image deconvolution [24, 26].

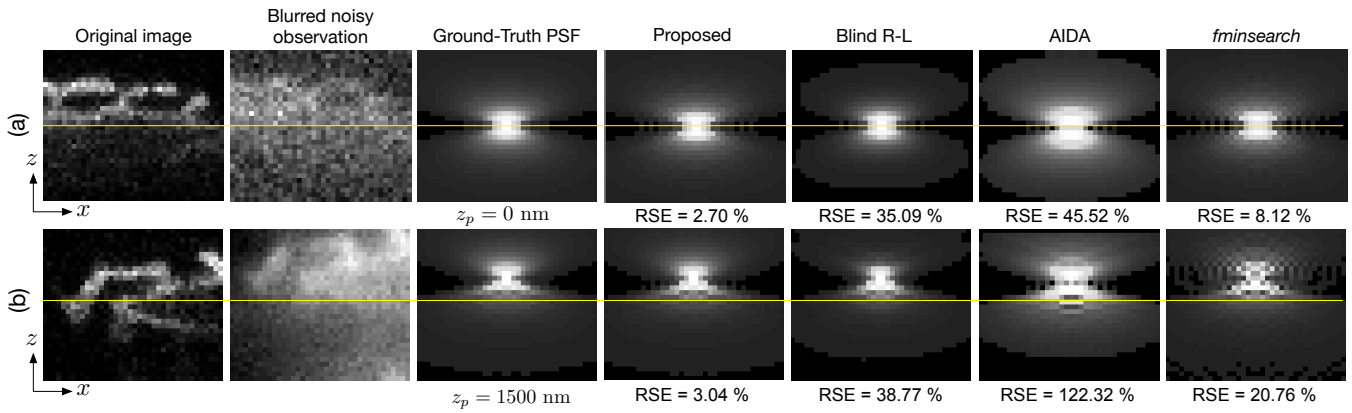

Fig. 2. Comparison results of PSF estimations. (a) the case of $z_p = 0\,\text{nm}, \alpha = 0.2, \sigma^2 = 0.2$; (b) the case of $z_p = 1500\,\text{nm}, \alpha = 0.02, \sigma^2 = 0.02$. $\lambda = 492\,\text{nm}$, NA = 1.4, $n_i = 1.33$ and $n_s = 1.4$. Locators (yellow line) indicate the location of displayed sections ($z = 0$). Images have been cropped and rescaled for visualization purpose.

6. REFERENCES

[1] M. Born and E. Wolf, *Principles of optics: electromagnetic theory of propagation, interference and diffraction of light*. Cambridge University Press, 1999.

[2] M. Arigovindan, J. C. Fung, D. Elnatan, V. Mennella, Y.-H. M. Chan, M. Pollard, E. Branlund, J. W. Sedat, and D. A. Agard, "High-resolution restoration of 3D structures from widefield images with extreme low signal-to-noise-ratio," *Proc. Natl. Acad. Sci.*, vol. 110, no. 43, pp. 17 344–17 349, 2013.

[3] P. Sarder and A. Nehorai, "Deconvolution methods for 3-D fluorescence microscopy images," *IEEE Signal Process. Mag.*, vol. 23, no. 3, pp. 32–45, 2006.

[4] D. Sage, L. Donati, F. Soulez, D. Fortun, G. Schmit, A. Seitz, R. Guiet, C. Vonesch, and M. Unser, "Deconvolutionlab2: An open-source software for deconvolution microscopy," *Methods*, vol. 115, pp. 28–41, 2017.

[5] J. Li, F. Luisier, and T. Blu, "PURE-LET deconvolution of 3D fluorescence microscopy images," in *Proc. IEEE Int. Symp. Biomed. Imaging (ISBI)*, 2017, pp. 723–727.

[6] S. F. Gibson and F. Lanni, "Experimental test of an analytical model of aberration in an oil-immersion objective lens used in three-dimensional light microscopy," *J. Opt. Soc. Am. A*, vol. 9, no. 1, pp. 154–166, 1992.

[7] P. Török and P. Varga, "Electromagnetic diffraction of light focused through a stratified medium," *Appl. Opt.*, vol. 36, no. 11, pp. 2305–2312, 1997.

[8] H. Kirshner, F. Aguet, D. Sage, and M. Unser, "3-D PSF fitting for fluorescence microscopy: implementation and localization application," *J. Microsc.*, vol. 249, no. 1, pp. 13–25, 2013.

[9] J. Li, F. Xue, and T. Blu, "Fast and accurate three-dimensional point spread function computation for fluorescence microscopy," *J. Opt. Soc. Am. A*, vol. 34, no. 6, pp. 1029–1034, 2017.

[10] A. S. Carasso, "APEX blind deconvolution of color Hubble space telescope imagery and other astronomical data," *Opt. Eng.*, vol. 45, no. 10, pp. 1–15, 2006.

[11] J. Markham and J.-A. Conchello, "Parametric blind deconvolution: a robust method for the simultaneous estimation of image and blur," *J. Opt. Soc. Am. A*, vol. 16, no. 10, pp. 2377–2391, 1999.

[12] T. Kenig, Z. Kam, and A. Feuer, "Blind image deconvolution using machine learning for three-dimensional microscopy," *IEEE Trans. Pattern Anal. Mach. Intell.*, vol. 32, no. 12, pp. 2191–2204, Dec. 2010.

[13] F. Soulez, L. Denis, Y. Tourneur, and É. Thiébaut, "Blind deconvolution of 3D data in wide field fluorescence microscopy," in *Proc. IEEE Int. Symp. Biomed. Imaging (ISBI)*, 2012, pp. 1735–1738.

[14] M. Keuper, T. Schmidt, M. Temerinac-Ott, J. Padeken, P. Heun, O. Ronneberger, and T. Brox, "Blind deconvolution of widefield fluorescence microscopic data by regularization of the optical transfer function (OTF)," in *Proc. IEEE Comput. Soc. Conf. Comput. Vis. Pattern Recognit. (CVPR)*, 2013, pp. 2179–2186.

[15] M. Tofighi, O. Yorulmaz, K. Köse, D. C. Yıldırım, R. Çetin-Atalay, and A. E. Cetin, "Phase and TV based convex sets for blind deconvolution of microscopic images," *IEEE J. Sel. Top. Signal Process.*, vol. 10, no. 1, pp. 81–91, 2016.

[16] F. Xue and T. Blu, "A novel SURE-based criterion for parametric PSF estimation," *IEEE Trans. Image Process.*, vol. 24, no. 2, pp. 595–607, 2015.

[17] J. Li, F. Xue, and T. Blu, "Gaussian blur estimation for photon-limited images," in *Proc. IEEE Int. Conf. Image Process. (ICIP)*, 2017, pp. 495–499.

[18] J. Li, F. Luisier, and T. Blu, "PURE-LET Image Deconvolution," *IEEE Trans. Image Process.*, vol. 27, no. 1, pp. 92–105, 2018.

[19] J. Boulanger, C. Kervrann, P. Bouthemy, P. Elbau, J.-B. Sibarita, and J. Salamero, "Patch-based nonlocal functional for denoising fluorescence microscopy image sequences," *IEEE Trans. Med. Imag.*, vol. 29, no. 2, pp. 442–454, 2010.

[20] B. Zhang, J. Zerubia, and J.-C. Olivo-Marin, "Gaussian approximations of fluorescence microscope point-spread function models," *Appl. Opt.*, vol. 46, no. 10, pp. 1819–1829, 1 Apr. 2007.

[21] E. F. Y. Hom, F. Marchis, T. K. Lee, S. Haase, D. A. Agard, and J. W. Sedat, "AIDA: an adaptive image deconvolution algorithm with application to multi-frame and three-dimensional data," *J. Opt. Soc. Am. A*, vol. 24, no. 6, pp. 1580–1600, Jun. 2007.

[22] S. Dmitrieff and F. Nédélec, "ConfocalGN: A minimalistic confocal image generator," *SoftwareX*, vol. 6, pp. 243–247, 2017.

[23] D. A. Fish, A. M. Brinicombe, E. R. Pike, J. G. Walker, and R. L. Algorithm, "Blind deconvolution by means of the Richardson-Lucy algorithm," *Appl. Opt.*, vol. 12, no. 1, 1995.

[24] B. Kim and T. Naemura, "Blind depth-variant deconvolution of 3D data in wide-field fluorescence microscopy," *Sci. Rep.*, vol. 5, p. 9894, 2015.

[25] J.-S. Lee, T.-L. E. Wee, and C. M. Brown, "Calibration of wide-field deconvolution microscopy for quantitative fluorescence imaging," *J. Biomol. Tech.*, vol. 25, no. 1, p. 31, 2014.

[26] N. Patwary and C. Preza, "Image restoration for three-dimensional fluorescence microscopy using an orthonormal basis for efficient representation of depth-variant point-spread functions," *Biomed. Opt. Express*, vol. 6, no. 10, pp. 3826–3841, 2015.